Dalton Transactions

ROYAL SOCIETY OF CHEMISTRY

PAPER

View Article Online
View Journal | View Issue

Cite this: *Dalton Trans.*, 2024, **53**, 14779

Optimizing post-synthetic metal incorporation in mixed-linker MOFs: insights from metalation studies on bipyridine-containing UiO-67 single crystals†

Wanja Gschwind, [a] Gyula Nagy, [b] Daniel Primetzhofer [b,c] and Sascha Ott *[a]

The postsynthetic metalation (PSM) of metal–organic frameworks (MOFs) with intrinsic metal binding sites is an intriguing strategy to introduce catalytic function into MOFs. The spatial distribution of the catalytic sites within the MOF crystal will affect the efficiency of the material, but the factors that govern depth distribution of the introduced metal sites are often not well understood. Herein, we employ Rutherford backscattering spectrometry (RBS) to investigate the metal distribution in a series of post-synthetically metalated mixed linker bpdc/BPY UiO-67 (UiO = Universitet i Oslo, bpdc = biphenyl-dicarboxylate, BPY = 2,2′-bipyridine-5,5′-dicarboxylate) single crystals as a function of linker ratio and metalation time. The RBS spectra reveal large differences in the depth distribution of inserted Ni^{2+} ions, and core/shell architectures are observed in high BPY materials at shorter incubation times. The incubation times to achieve uniform metal incorporation increases with increasing BPY ratios in the materials, suggesting that the presence of the BPY linkers slow down metal uptake. We propose a combination of ionic interactions and pore clogging, where coordinated ions reduce the available pore space for further ions to diffuse deeper into the framework as reasons for the observed trends. The observations are likely relevant for other mixed-linker MOF systems, and understanding the effect that linker ratios have on PSM and cation distribution will aid in future optimizations of catalytic MOFs.

Received 19th June 2024,
Accepted 9th August 2024

DOI: 10.1039/d4dt01782j

rsc.li/dalton

Introduction

Metal organic frameworks (MOFs) are a class of highly versatile materials for a variety of applications, ranging from carbon capture,[1] storage,[2] sensing,[3] separation,[4] biomedicine,[5] to catalysis.[6] In terms of catalytic applications, MOFs have generally been recognized as highly potent support materials for the heterogenization of molecular catalysts.[6–11] They offer structural control, tunable environments, and high internal surface areas, making them promising host materials for catalytic processes, with potential applications in green chemistry and renewable fuel production.[10,12]

A popular approach for the production of such MOF-catalyst hybrid materials is *via* post-synthetic metalation (PSM).[13–15] In this procedure, catalytically active metal cations are introduced into pre-formed MOF crystals that contain suitable anchoring sites. A common design strategy is to have the anchoring site on the linker, such as in free base porphyrinic MOFs or UiO-67 analogues with BPY linkers (BPY = 2,2′-bipyridine-5,5′-dicarboxylate).[16] During PSM, MOF crystals are soaked in a solution of the desired metal ions, allowing the latter to diffuse into the porous material and to bind to the anchoring sites. Understanding the movement of metal ions through the MOF is important for the optimization of the metalation step because the spatial distribution of the catalytic sites will strongly influence the catalytic efficiency of the materials. Several factors are expected to influence the depth profile of the introduced metal centers, such as metalation time, temperature, solvent, but also the nature of the metal ion and the structure of the MOF.

MOFs that are composed of zirconium-based secondary building units (SBUs) are known for their thermal, chemical, and mechanical stability.[17,18] One prominent example is the UiO MOF series, which is based on Zr-oxo clusters that are linked by carboxylate-terminated organic linkers.[19,20] Within this series, UiO-66 and UiO-67 are the most widely used structures and have been modified in many ways to enable the

[a]*Department of Chemistry – Ångström Laboratory, Uppsala University, Box 523, 751 20 Uppsala, Sweden. E-mail: sascha.ott@kemi.uu.se*
[b]*Department of Physics and Astronomy, Uppsala University, Box 516, 751 20 Uppsala, Sweden*
[c]*Tandem Laboratory, Uppsala University, Box 529, 751 20 Uppsala, Sweden. E-mail: daniel.primetzhofer@physics.uu.se*

† Electronic supplementary information (ESI) available. See DOI: https://doi.org/10.1039/d4dt01782j

incorporation of molecular catalysts.[19,21] As many established metal catalysts feature a bipyridine moiety coordinating to the metal center, this structure was introduced into UiO-67 by exchanging a fraction of the native biphenyl-dicarboxylate (bpdc) linkers for BPY linkers. The resulting UiO-67-BPY has been extensively used for the incorporation of metal catalysts and produced promising catalytic systems.[13,22] One additional benefit of such a MOF is the tunability obtained by varying the ratio between the original linker and linker with the coordination site.[23] This variation will impact the catalyst concentration in the MOF, but can also influence framework stability[23] or mass- and charge transport[24,25] phenomena within the framework.

Many catalytic MOF materials use such a mixed linker system, where a fraction of the linkers contains an anchoring site for catalyst binding.[23] In those mixed linker materials, the overall topology is assumed to remain unchanged, regardless of the linker ratio. What has been neglected so far is how the ratio of different linker types influences the spatial distribution of post-synthetically introduced metal sites. This is important, because ions that enter crystals with high contents of metal binding sites experience different chemical environments compared to those that diffuse into MOFs with few binding sites (Fig. 1).

Herein, we synthesized a series of mixed linker UiO-67-BPY single crystals containing different proportions of bpdc and BPY linkers, and post-synthetically metalated them for varying amounts of time. To investigate the effect of the linker ratio on the diffusion of the metal ions, we studied the spatial distribution of metal ions in UiO-67-BPY single crystals by micro-Rutherford backscattering spectrometry (RBS). This method allows the determination of elemental depth profiles in individual MOF single crystals, providing information on post-synthesis metal distribution.[26]

Results & discussion

UiO-67-BPY single crystals containing varying ratios of BPY and bpdc linker (100, 50, 30 and 15% BPY, subsequently written as UiO-67-BPY$_{xx\%}$) were grown on Si substrates using a modified version of our previous procedure.[26] In short, a precursor solution was prepared from a mixture of 2,2′-bipyridine-5,5′-dicarboxylate and biphenyl-dicarboxylate (0.2 mmol combined), benzoic acid (1.85 g, 15.2 mmol), $ZrCl_4$ (87.4 mg, 0.4 mmol), and 24 μL water in anhydrous DMF (15 mL). Washed Si slides were placed face down at a tilt angle inside 4 mL glass vials, and covered by 2 mL precursor solution. The vials were sealed with septa containing caps, placed in a sand bath and transferred to an oven preheated to 120 °C for 5 days. After removal from the oven, the wafers were washed and stored in DMF. Prior to analysis, the solvent was exchanged to acetone and the substrates were dried under vacuum.

Successful MOF synthesis was confirmed by X-ray diffraction (XRD) and scanning electron microscopy (SEM). The representative XRD graph (Fig. 2a) shows the presence of the characteristic UiO-67 ⟨111⟩ and ⟨222⟩ reflections (black line), confirming the presence of crystalline UiO-67-type materials. The absence of the remaining peaks that are present in the simulation for bulk powder UiO-67 (red line) confirms the high orientation of the surface-grown crystals. The SEM image (Fig. 2b) shows a well separated single crystal of *circa* 15 μm diameter, in the characteristic shape of UiO-67 octahedra grown in a ⟨111⟩ orientation.

To confirm the linker composition of the materials, the synthesized MOF crystals were digested in aqueous NaOD (see ESI†) and subjected to NMR analysis (Fig. 3). From the resulting NMR spectra, the bpdc:BPY ratios in the mixed linker MOF could be calculated and related to the feeding ratio of the two linkers in the solvothermal syntheses.

The results show a satisfactory match between the feeding ratio and the linker ratio in the MOF. There likely is no preference for either one or the other linker during the mixed linker synthesis. This finding also implies that a statistical distribution of both linkers within a single MOF crystal can be expected. This assumption is further supported by the fact that UiO-67 has been shown to undergo post-synthetic linker exchange with exogenously added BPY, meaning that there is a pathway to equilibrate any potential inhomogeneities in the mixed linker MOF under the solvothermal reaction conditions.[19,21]

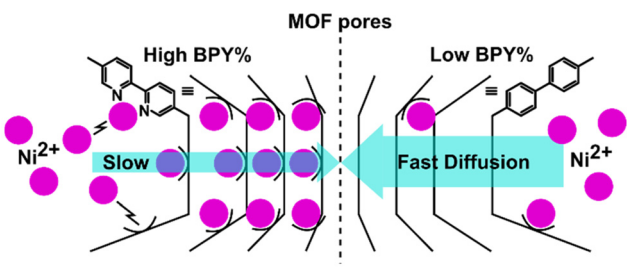

Fig. 1 Schematic representation of Ni^{2+} cations entering a MOF with high (left) and low (right) BPY content.

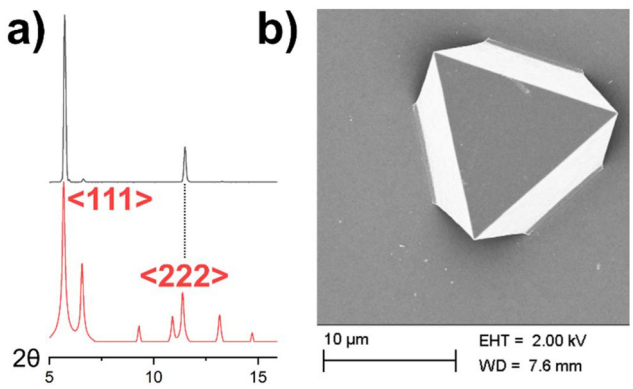

Fig. 2 (a) In black, a measured XRD pattern of synthesized UiO-67-BPY$_{100\%}$ crystals displaying only the ⟨111⟩ and ⟨222⟩ reflections; in red a simulated XRD spectrum of non-oriented UiO-67 crystals. (b) SEM picture of a synthesized UiO-67-BPY$_{100\%}$ crystal on a Si substrate.

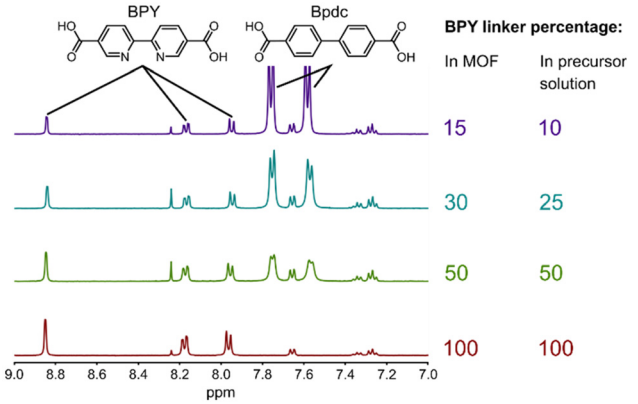

Fig. 3 NMR spectra of digested UiO-67 crystals containing different percentages of BPY linker. The table shows the BPY percentage in the precursor solution compared to the measured BPY percentage in the digested MOF crystals. BPY percentage values were rounded to multiples of 5.

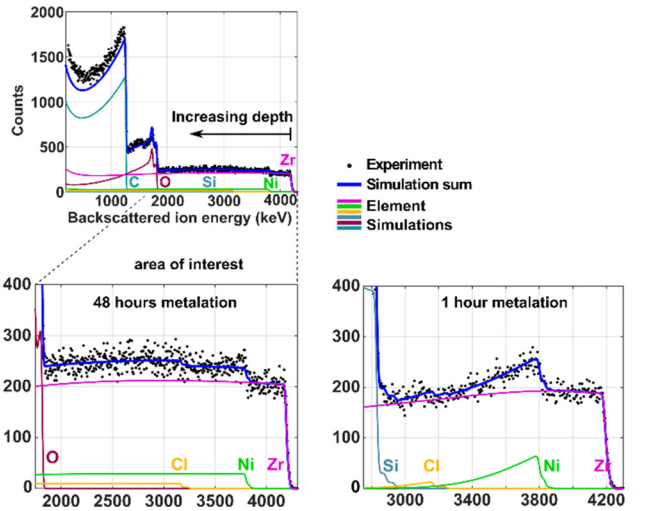

Fig. 4 RBS spectra (5 MeV He ion beam) of metalated UiO-67-BPY single crystals containing 30% BPY, incubated in 4 mM solution of Ni^{2+} in DMF for 1 and 48 hours.

For the post-synthetic metalation, the wafers were rinsed to remove loosely bound precursor components, and transferred directly into the metalation solution. More specifically, the metalation was studied using Ni^{2+} (4 mM $NiCl_2$ in DMF) as cation of choice. This is motivated by the fact that $[Ni(BPY)]^{2+}$ – type species are prominent redox catalyst for a variety of transformations.[27–30] The metalation process was then performed at 100 °C for a specified amount of time. The retention of structure and crystallinity during PSM was confirmed by X-ray diffraction (Fig. S1†). Further support for the structural integrity of the samples was obtained from SEM which showed unaltered crystal morphologies after PSM (Fig. S2†).

For the investigation of post-synthetic metal distribution, the metalated crystals were analyzed by RBS.[31] For such measurements, a continuous beam of He ions of known energy is focused onto the sample where the individual ions can get backscattered from encountered target atoms. The energy of the backscattered He ion is related to the mass of the encountered atom in the sample, and to the depth in which the collision occurred. From this data, element specific depth profiles for the encountered atoms can be constructed. A representative RBS spectrum is presented in Fig. 4 in which the experimental data (in black), obtained from a 5 MeV He ion beam, is fitted using the SIMNRA software package (blue line).[32] The *Y*-axis presents the number of back-scattered ions of a specific energy, which depends on the concentration of the elements that have contribution to this specific energy. The *X*-axis displays the energy of the backscattered ions which is dependent on the mass of the encountered nucleus, and also on the depth, at which the nucleus was encountered. Therefore, heavier elements, and atoms at the surface of the crystal, both produce higher energy signals compared to lighter elements or atoms deeper within the sample, respectively.

With diffusion being a time dependent phenomenon, it is intuitive to assume that metalation time will impact the depth distribution of Ni^{2+} in UiO-67-BPY single crystals, as well as its total incorporation yield. Thus, two samples of UiO-67-$BPY_{30\%}$ were incubated in a Ni^{2+} containing solution for 1 and 48 hours. RBS spectra were measured to reveal the Ni^{2+} distribution within the metalated crystals (Fig. 4). The region of interest (lower part of Fig. 4) depicts the energy range containing the Zr and Ni signals. The highest energy signal results from ions scattering off the heaviest element found on the surface of the sample – in this case Zr. Moving towards lower energies, the detected ions have traveled deeper into the crystal before scattering off a Zr nucleus. The number of counts remains constant in this part of the spectrum, indicating a constant Zr concentration. At approximately 3800 keV, an increase in the number of counts is observed. According to the kinematic equation, this increase in counts results from surface Ni^{2+} and not from a sudden increase in Zr at a certain depth.[33] The Ni signal lies on top of the Zr signal, but the two signals can be separated assuming that the Zr concentration remains constant throughout the crystal. Again, towards lower energy, the signals from Ni^{2+} at increasing crystal depth is observed. It is here that the two spectra in Fig. 4 start to differ. The spectrum after 48 hours metalation depicts a constant Ni count with increasing probing depth, indicating a constant Ni^{2+} concentration throughout the probed layer. The 1 hour metalated sample, however, exhibits a distinct decrease of the Ni signal with increasing probing depth. At lower energies, the count number stabilizes at the height of the Zr signal, suggesting the absence of Ni^{2+} below a certain depth. This indicates a concentration gradient from elevated Ni^{2+} concentrations near the crystal surface towards minimal Ni^{2+} content in the crystal core. The horizontal (energetic) distance between the appearance of the Ni signal and its disappearance can be used to calculate the thickness of the layer containing Ni (*vide infra*). The observed Ni concentration gradient is a direct

result of the diffusion of Ni^{2+} through the crystal pores. These spectra, therefore, aptly demonstrate the critical role of time for PSM, visualizing the time dependent progression of the diffusion layer within the crystal.

At lower energies, signals from the lighter elements such as the Si substrate, carbon from the linkers and oxygen form the SBUs can be observed. The count numbers of these elements are however highly dependent on elastic resonances, and cannot be used to visually deduct any information on elemental concentrations.

In a second set of experiments, the correlation between the Ni^{2+} uptake and the percentage of BPY linker was investigated. Since the BPY linker bears the anchoring site for Ni^{2+}, higher Ni^{2+} concentrations are expected in a crystal with higher BPY percentage. Therefore, three mixed linker UiO-67-BPY samples containing different BPY percentage (approximately 15, 30, and 50%) were analyzed by RBS and compared (Fig. 5).

All three RBS spectra show a constant Zr and Ni^{2+} concentration throughout the probed depth. When comparing the spectra, a higher Ni edge is observed with increasing BPY linker percentage, indicating a higher Ni : Zr ratio in the crystal. A perfect crystal model would be comprised of 6 organic linkers per $Zr_6O_4(OH)_4$ cluster, resulting in a linker to Zr ratio of 1 : 1. In case of a stoichiometric metalation process, each BPY linker would coordinate one Ni^{2+} ion, leading to a Ni : Zr ratio that corresponds exactly to the BPY percentage. Looking at the table of extracted Ni : Zr ratios (Fig. 5), it becomes apparent that the ratios are slightly higher than expected based on that ideal model, suggesting some excess Ni^{2+} being adsorbed in the MOF pores. This extra population could be due to interactions with coordinatively unsaturated SBUs or the formation of Cl^- or H_2O bridged $(Ni^{2+})_2$ complexes, both of which have precedence in the literature.[34–37] Despite of this complication, the data clearly confirms a correlation between the BPY percentage and Ni^{2+} uptake.

While the BPY percentage dictates the maximum amount of Ni^{2+} that can be coordinated within the framework, Fig. 4 shows that the incorporation yield and depth distribution of PSM strongly depends on metalation time. This strong time dependence is because metalation is mostly dictated by two factors: the speed with which the introduced metal precursor diffuses into the crystal, and how fast it coordinates to the BPY linkers.[38] There is though a lack of research on how the BPY percentage influences the metal distribution. That is by changing the MOF pore environment enough to cause a notable change in diffusion processes and thereby relating metalation time to linker ratio.

To assess the impact of varying linker ratios in mixed linker MOFs, UiO-67-BPY single crystals with different BPY percentages were metalated for either 1 or 24 hours. Subsequent analysis using RBS was used to reveal the distribution of Ni^{2+} within each sample (Fig. 6).

Comparison of the shape and size of the Ni signals between the spectra within the same column in Fig. 6, visualizes the influence of the incubation time on the Ni^{2+} distribution in a UiO-67 crystal with a specific BPY linker concentration. At 100% BPY after 1 hour of incubation, a very small and rapidly decaying Ni signal is observed, suggesting Ni^{2+} incorporation only in the surface regions (0.3 μm) of the crystal. After 24 hours of incubation, the Ni signal is much more pronounced and declines less rapidly. Higher concentrations of Ni^{2+} ions are thus detected deeper within the crystal, indicating higher Ni^{2+} uptake and farther diffusion (2.7 μm) into the crystal, but still not reaching the crystal core. In contrast, the materials with a low BPY content exhibit relatively comparable Ni^{2+} distributions after both 1 and 24 hours of incubation. This observation implies that, at lower BPY percentage, the relevance of metalation time diminishes, indicating a significantly accelerated Ni^{2+} diffusion in lower BPY materials. The pronounced difference in the Ni signals at high BPY percentages, however, suggests that incubation time has a strong impact on the resulting Ni^{2+} distribution. Evaluating these findings across all materials reveals a clear trend, showing that the higher the BPY percentage of the material the more important the metalation time becomes.

Comparing the spectra of Fig. 6 horizontally, the effect of the BPY:bpdc ratio can be observed. Looking at the spectrum of 100% BPY, 24 h, a pronounced slope in the Ni signal can be observed, indicating a rapid decline of the Ni^{2+} concentration towards the crystal core. In contrast, at 15% BPY, 24 h, the Ni signal runs parallel to the underlying Zr baseline, indicating a uniform Ni^{2+} concentration throughout the probed depth. Comparing the Ni slopes of samples incubated for the same duration provides information on the relationship between the BPY ratio and the Ni^{2+} distribution. A clear trend is observed, showing a more pronounced Ni^{2+} concentration gradient towards high BPY percentages and more uniform metalation towards low BPY percentages. These differences in the Ni^{2+} distribution seem to be a direct result of the different BPY:bpdc ratios in the analyzed crystals. This supports our previous conclusion, suggesting a diminished Ni^{2+} diffusion rate in high BPY frameworks.

The Ni^{2+} ions diffusing into the framework experience different environments when moving through MOFs with varying amounts of BPY binding sites. A material featuring high BPY concentration will offer many coordination opportu-

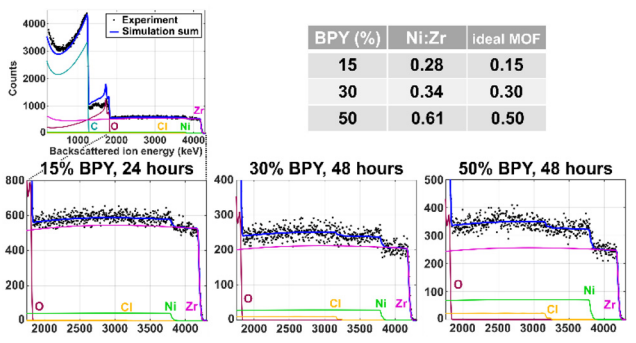

BPY (%)	Ni:Zr	ideal MOF
15	0.28	0.15
30	0.34	0.30
50	0.61	0.50

Fig. 5 RBS spectra of UiO-67-BPY single crystals containing different BPY percentages. Table showing the extracted Ni : Zr ratios.

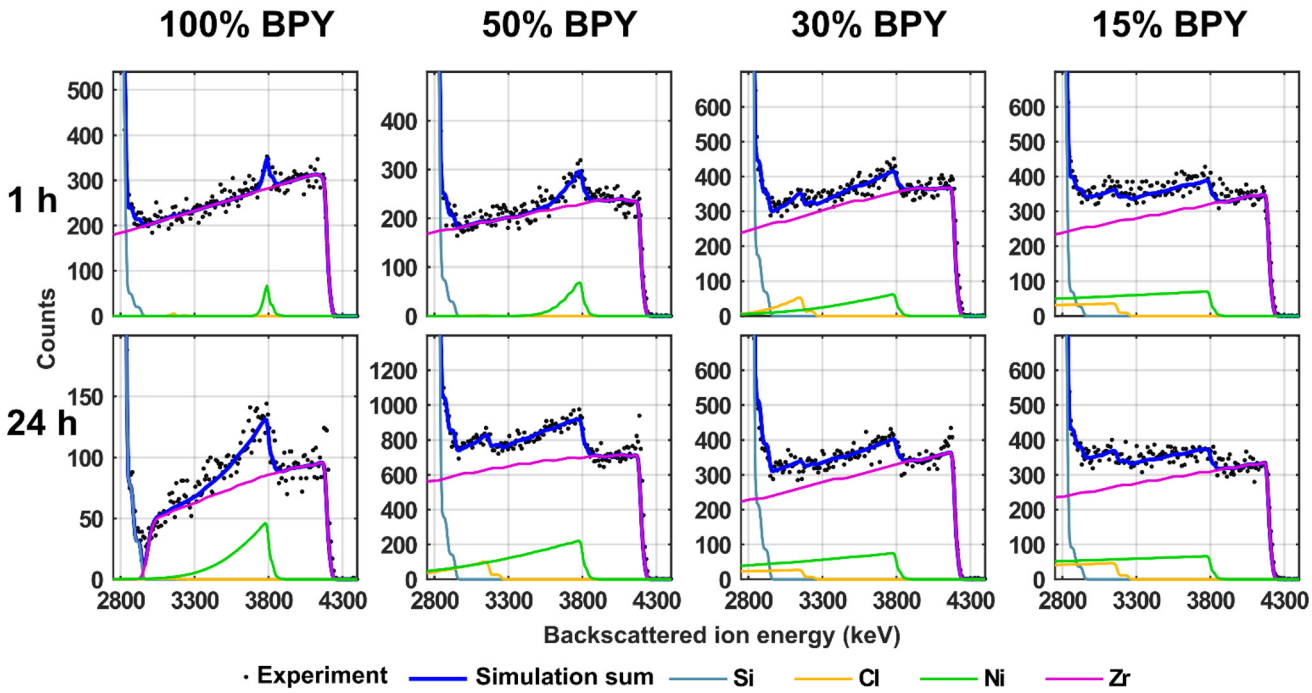

Fig. 6 RBS spectra of Ni^{2+}-metalated UiO-67-BPY single crystals with varying percentages of BPY linker, metalated for 1 or 24 hours.

nities to incoming ions, also resulting in a high number of interactions between the framework and the ions. If coordination is fast compared to diffusion, subsequent Ni^{2+} ions move through pores filled with high concentrations of coordinated Ni^{2+}. In contrast, when moving through a low BPY material, the linker–ion interactions and coordination opportunities are fewer, and subsequent Ni^{2+} ions do not encounter high concentrations of coordinated Ni^{2+}.

From this, two plausible factors may account for the slower Ni^{2+} diffusion in high BPY materials. Firstly, interactions between diffusing Ni^{2+} ions and the bipyridine anchoring sites are expected to slow down diffusion.[39] The attracting forces between the opposing charges of the Ni^{2+} ions and the electron lone pairs on the non-coordinated nitrogen atoms will slow down the movement of Ni^{2+} ions through the material. Therefore, an increasing BPY ratio would increase the frequency of such interactions, and slow down diffusion. Secondly, diffusion is susceptible to steric hindrance, which is highly relevant when a species is diffusing through the narrow pores of a MOF.[39] With the binding of a Ni^{2+} ion to an open coordination site on a BPY linker, we expect a concomitant reduction of the available pore space for subsequent Ni^{2+} ions. Consequently, as the ratio of BPY linker and coordinated Ni^{2+} ions increases, the available pore space is reduced, notably hindering diffusion into deeper regions of the crystal.

Another noteworthy phenomenon observed in the RBS spectra following extended incubation time (24 h, 100–30% BPY), is the appearance of a pronounced peak at the high energy edge of Zr (4150 keV). Such an increased Zr signal at the high energy edge indicates higher Zr concentration at the crystal surface, which suggests the accumulation of Zr at the surface. This phenomenon also appears to correlate with the BPY percentage. Prior investigations of UiO-67 MOFs have indicated the possibility of partial structural degradation due to hydrolysis.[40] Some studies also observed accelerated hydrolysis in the presence of BPY linkers, which act as base to deprotonate incoming water molecules, thereby accelerating the hydrolysis of the linker–Zr bonds.[41] The observed accumulation of Zr may therefore be rationalized by a moisture induced structural collapse of the outer crystal layers, resulting in the formation of a denser and amorphous layer of Zr and linker. The presence of such a layer is expected to impede the ingress of material into and out of the crystal, possibly being another factor that contributes to diminished Ni^{2+} incorporation.[39] Moreover, surface collapse is likely to influence the washing procedure as well, slowing down the removal of non-specifically adsorbed Ni^{2+} and thus providing another potential explanation for the superstoichiometric amounts of Ni^{2+} within the crystals.

The information obtained through the fitting of the RBS spectra enables the calculation of diffusion coefficients.[42] A simple Fickian diffusion function was used to plot curves for each diffusion coefficient extracted from the measured crystals, enabling the visualization and comparison of Ni^{2+} diffusion in the different materials (Fig. 7).

Fig. 7 nicely visualizes the substantial influence of the BPY-linker percentage on metal diffusion within the frameworks. For the 15% BPY crystal, an almost uniform Ni^{2+} distribution can be observed after only 1 hour metalation, while, in contrast, the 100% BPY crystal shows only near surface metal uptake. The formal diffusion coefficients (c) differ by orders of magnitude depending on the BPY ratio of the mixed-linker

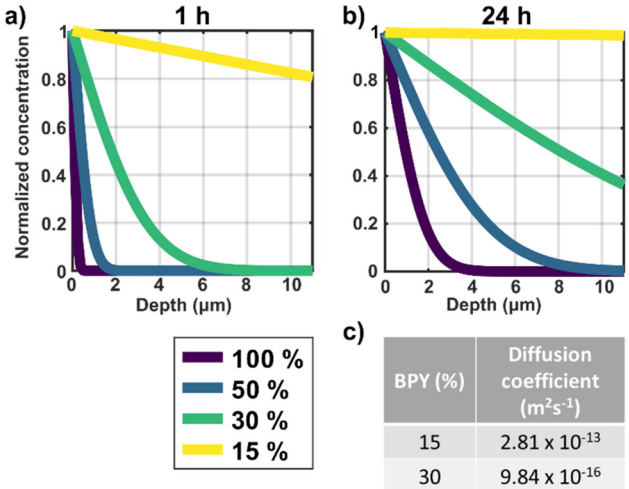

c)

BPY (%)	Diffusion coefficient (m^2s^{-1})
15	2.81×10^{-13}
30	9.84×10^{-16}
50	5.87×10^{-17}
100	3.51×10^{-18}

Fig. 7 Depth-dependent Ni^{2+} concentration in four mixed-linker UiO-67-BPY MOFs (15–100% BPY) after (a) 1 hour, and (b) 24 hours metalation. The graphs were obtained by plotting diffusion functions using the different diffusion coefficients presented in (c) table of Fickian Ni^{2+} diffusion coefficients extracted from fitting the RBS spectra of the different mixed-linker crystals metalated for one hour (from Fig. 6).

MOF. Such tables and graphs greatly facilitate the comparison of the metal diffusion during PSM under different conditions, and help us understand metal distribution in post-synthetically metalated MOF crystals.

Conclusions

The Ni^{2+} distribution in a series of post-synthetically metalated UiO-67-BPY MOFs containing various ratios of BPY linker (100, 50, 30, and 15%) was investigated by RBS. The resulting spectra revealed new information, relating the Ni^{2+} distribution to the BPY percentage and metalation time. As expected, the total Ni^{2+} uptake correlates with the ratio of BPY linkers, which act as coordination sites for the incoming metal ions, allowing the framework to take up higher amounts of Ni^{2+} with increasing BPY linker content. Furthermore, since PSM relies on diffusion of the Ni^{2+} ions into the MOF, the uptake of Ni^{2+} and its distribution within the crystals is naturally influenced by the metalation time. This time dependence is clearly visible in the analyzed spectra. However, the analyzed series also revealed a strong link between the BPY percentage of a material and the Ni^{2+} diffusion. The spectra point to a significantly slower Ni^{2+} diffusion in high BPY materials, suggested by a Ni^{2+} distribution only near the crystal surface. In contrast, the low BPY materials showed much faster Ni^{2+} uptake and uniform distribution of the Ni^{2+} throughout the crystal.

Longer incubation time of high BPY crystals enables higher and deeper Ni^{2+} incorporation but possibly at the cost of structural degradation of the surface layers. This was indicated by the appearance of higher Zr concentrations at the crystal surface, signifying a layer of more densely packed Zr structures at the surface, suggesting a collapse of the pores.

The slower Ni^{2+} diffusion related to higher BPY linker percentage revealed in this work could be related to an increasing amount of polar interactions between the linkers and the diffusing Ni^{2+} ions. Another reason could be that coordinated Ni^{2+} decreases available pore space that is needed for subsequent Ni^{2+} to diffuse through the framework, resulting in a clogging effect, when the amount of BPY linker and coordinated Ni^{2+} gets too high.

Furthermore, the fitting of the spectra enables the extraction of quantitative values of formal Ni^{2+} diffusion coefficients. This approach enables visual representations of metal distribution in post-synthetically metalated MOFs, aiding the understanding and comparisons of these systems. Such comparisons further enable discussions on the efficiency of the synthesized materials and may offer pathways to improvement. The use of RBS as a technique to obtain depth profiles of introduced metal ions is by no means limited to the MOFs used herein. The findings are likely to be relevant for other mixed linker MOF systems, and could help future research choosing specific linker ratios to optimize catalyst loading in such hybrid materials.

Author contributions

Wanja Gschwind: conceptualisation, investigation, resources, visualization, writing – original draft, writing – review & editing. Gyula Nagy: formal analysis, investigation, methodology, visualization, writing – review & editing. Daniel Primetzhofer: funding acquisition, supervision, writing – review & editing. Sascha Ott: conceptualisation, funding acquisition, supervision, writing – review & editing.

Data availability

Additional data supporting this article have been included as part of the ESI.† Numerical data can be made available upon request.

Conflicts of interest

There are no conflicts to declare.

Acknowledgements

Support from the Swedish Research Council (2023-03395), the Swedish Energy Agency (42029-2), and VR-RFI (2019_00191) for the Accelerator-based ion-technological center for the Tandem Accelerator Laboratory in Uppsala University is acknowledged.

References

1 M. Ding, R. W. Flaig, H. L. Jiang and O. M. Yaghi, *Chem. Soc. Rev.*, 2019, **48**, 2783–2828.
2 Y. H. Hu and L. Zhang, *Adv. Mater.*, 2010, **22**, E117–E130.
3 P. Kumar, A. Deep and K.-H. Kim, *TrAC, Trends Anal. Chem.*, 2015, **73**, 39–53.
4 Y. Wang and D. Zhao, *Cryst. Growth Des.*, 2017, **17**, 2291–2308.
5 S. Keskin and S. Kızılel, *Ind. Eng. Chem. Res.*, 2011, **50**, 1799–1812.
6 A. Bavykina, N. Kolobov, I. S. Khan, J. A. Bau, A. Ramirez and J. Gascon, *Chem. Rev.*, 2020, **120**, 8468–8535.
7 Y.-S. Kang, Y. Lu, K. Chen, Y. Zhao, P. Wang and W.-Y. Sun, *Coord. Chem. Rev.*, 2019, **378**, 262–280.
8 J. Liu, L. Chen, H. Cui, J. Zhang, L. Zhang and C. Y. Su, *Chem. Soc. Rev.*, 2014, **43**, 6011–6061.
9 A. H. Chughtai, N. Ahmad, H. A. Younus, A. Laypkov and F. Verpoort, *Chem. Soc. Rev.*, 2015, **44**, 6804–6849.
10 M. B. Majewski, A. W. Peters, M. R. Wasielewski, J. T. Hupp and O. K. Farha, *ACS Energy Lett.*, 2018, **3**, 598–611.
11 Q. Wang and D. Astruc, *Chem. Rev.*, 2020, **120**, 1438–1511.
12 N. F. Suremann, B. D. McCarthy, W. Gschwind, A. Kumar, B. A. Johnson, L. Hammarstrom and S. Ott, *Chem. Rev.*, 2023, **123**, 6545–6611.
13 R. Li, X. Li, D. Ramella, Y. Zhao and Y. Luan, *New J. Chem.*, 2022, **46**, 5839–5847.
14 S. M. Cohen, *Chem. Rev.*, 2012, **112**, 970–1000.
15 S. M. Cohen, *J. Am. Chem. Soc.*, 2017, **139**, 2855–2863.
16 K. Manna, T. Zhang and W. Lin, *J. Am. Chem. Soc.*, 2014, **136**, 6566–6569.
17 Z. Chen, S. L. Hanna, L. R. Redfern, D. Alezi, T. Islamoglu and O. K. Farha, *Coord. Chem. Rev.*, 2019, **386**, 32–49.
18 Y. Bai, Y. Dou, L. H. Xie, W. Rutledge, J. R. Li and H. C. Zhou, *Chem. Soc. Rev.*, 2016, **45**, 2327–2367.
19 A. H. Vahabi, F. Norouzi, E. Sheibani and M. Rahimi-Nasrabadi, *Coord. Chem. Rev.*, 2021, **445**, 214050.
20 S. J. Jasmina Hafizovic Cavka, U. Olsbye, N. Guillou, C. Lamberti, S. Bordiga and K. P. Lillerud, *J. Am. Chem. Soc.*, 2008, **130**, 2.
21 B. A. Johnson, A. Bhunia and S. Ott, *Dalton Trans.*, 2017, **46**, 1382–1388.
22 T. N. Tu, M. V. Nguyen, H. L. Nguyen, B. Yuliarto, K. E. Cordova and S. Demir, *Coord. Chem. Rev.*, 2018, **364**, 33–50.
23 A. Dhakshinamoorthy, A. M. Asiri and H. Garcia, *Catal. Sci. Technol.*, 2016, **6**, 5238–5261.
24 D. U. Satoshi Horike and S. Kitagawa, *Acc. Chem. Res.*, 2012, **46**, 9.
25 B. A. Johnson, A. M. Beiler, B. D. McCarthy and S. Ott, *J. Am. Chem. Soc.*, 2020, **142**, 11941–11956.
26 B. D. McCarthy, T. Liseev, M. A. Sortica, V. Paneta, W. Gschwind, G. Nagy, S. Ott and D. Primetzhofer, *J. Am. Chem. Soc.*, 2021, **143**, 18626–18634.
27 Y. Rollin, M. Troupel, D. G. Tuck and J. Perichon, *J. Organomet. Chem.*, 1986, **303**, 7.
28 S. Sengmany, S. Vasseur, A. Lajnef, E. Le Gall and E. Léonel, *Eur. J. Org. Chem.*, 2016, **2016**, 4865–4871.
29 S. Sengmany, A. Vitu-Thiebaud, E. Le Gall, S. Condon, E. Leonel, C. Thobie-Gautier, M. Pipelier, J. Lebreton and D. Dubreuil, *J. Org. Chem.*, 2013, **78**, 370–379.
30 S. T. Madrahimov, J. R. Gallagher, G. Zhang, Z. Meinhart, S. J. Garibay, M. Delferro, J. T. Miller, O. K. Farha, J. T. Hupp and S. T. Nguyen, *ACS Catal.*, 2015, **5**, 6713–6718.
31 G. Nagy, H. J. Whitlow and D. Primetzhofer, *Nucl. Instrum. Methods Phys. Res., Sect. B*, 2022, **533**, 66–69.
32 M. Mayer, *Report IPP* 9/113, 1997.
33 C. Jeynes, N. P. Barradas and E. Szilagyi, *Anal. Chem.*, 2012, **84**, 6061–6069.
34 B. Brewer, N. R. Brooks, S. Abdul-Halim and A. G. Sykes, *J. Chem. Crystallogr.*, 2003, **33**, 11.
35 D. L. Reger, A. E. Pascui, P. J. Pellechia, M. D. Smith, J. Jezierska and A. Ozarowski, *Inorg. Chem.*, 2014, **53**, 4325–4339.
36 R. J. Butcher and E. Sinn, *Inorg. Chem.*, 1977, **16**, 10.
37 S.-H. Liu, S.-Y. Li, L.-H. Wang, Q.-Z. Xu, R.-L. Zhang and C.-G. Cheng, *Z. Kristallogr.*, 2014, **229**, 2.
38 J. A. Boissonnault, A. G. Wong-Foy and A. J. Matzger, *J. Am. Chem. Soc.*, 2017, **139**, 14841–14844.
39 C. H. Sharp, B. C. Bukowski, H. Li, E. M. Johnson, S. Ilic, A. J. Morris, D. Gersappe, R. Q. Snurr and J. R. Morris, *Chem. Soc. Rev.*, 2021, **50**, 11530–11558.
40 N. C. Burtch, H. Jasuja and K. S. Walton, *Chem. Rev.*, 2014, **114**, 10575–10612.
41 J. B. DeCoste, G. W. Peterson, H. Jasuja, T. G. Glover, Y.-g. Huang and K. S. Walton, *J. Mater. Chem. A*, 2013, **1**, 5642–5650.
42 G. Nagy, W. Gschwind, S. Ott and D. Primetzhofer, Evaluating non-destructive quantification of composition gradients in metal-organic frameworks by MeV ion microbeam analysis, submitted manuscript, 2024.